An Eddy-Resolving Numerical Model of the Ventilated Thermocline: Time Dependence

MICHAEL D. COX

Geophysical Fluid Dynamics Laboratory/NOAA, Princeton University, Princeton, NJ 08542

(Manuscript received 25 August 1986, in final form 30 December 1986)

ABSTRACT

A primitive equation, eddy-resolving numerical model is used to study the inherent time scales of variability in the subtropical ocean, assuming temporally constant surface forcing. Three primary scales arise: mesoscale variability of roughly 50-day period, zonally elongated barotropic bands of 1.1-year period, and basin-scale undulations of approximately 4-year period. The latter are identified as first baroclinic mode Rossby waves, associated with bursts of ventilation at isopycnal outcrops. As a result, the equatorward transport required by Sverdrup theory in the subtropics occurs not as a broad, sluggish drift throughout the interior, but as a succession of more intense flows that slowly propagate westward.

The zonally elongated bands agree in characteristics to those predicted from theory of homogeneous turbulence. Eddy energy that is generated by baroclinic instability leaks from baroclinic to barotropic mode and thereafter, due to rotational constraints, seeks low zonal wavenumbers. The group velocity of the zonal bands is such that they tend to concentrate in the western interior of the subtropical gyre. The resulting anisotropy in eddy energy produces stronger zonal than meridional mixing by eddy processes in the model.

1. Introduction

The study of variability within the circulation and water mass properties of the oceans has proceeded, in recent decades, at quite different rates, depending upon the time scales involved. This is due, in large part, to the development of new techniques of measurement which have produced types of datasets that were previously unavailable. The ability to acquire synoptic data over larger spans of space and time has enabled a rapidly growing wealth of information in recent years on the character of mesoscale eddies and the role they play in the dynamics of the oceanic circulation. See Robinson (1983) for a survey of this work. The combination of old and new observations of the water masses of the deep ocean (e.g., Roemmich and Wunsch, 1984) has improved our knowledge of the long time-scale behavior there.

It remains quite difficult, however, to observe phenomena that require synoptic analysis and also possess time scales longer than several months. Examples of the type of data needed for this analysis are the Panulirus data from near Bermuda that extends over a period of more than thirty years, and datasets from several ocean weather station ships. An alternative approach is to use a combination of all available hydrographic data to infer time dependent phenomena over a region. An example is the work of Price and Magaard (1980) who have conducted such a study for the North Pacific and found evidence for long baroclinic Rossby waves of 2–10 year period. White and Saur (1983) have suggested that these waves are primarily driven by wind fluctuations either directly or via telecommunication by Kelvin waves along the eastern boundary carrying signals from wind-driven tropical disturbances.

The purpose of the present investigation is to evaluate the scales of time dependence that arise in an eddy resolving numerical model that are longer than those usually associated with mesoscale eddies. Holland (1978), evaluating solutions from a quasi-geostrophic eddy resolving model, reports considerable energy in time-dependent fluctuations of period greater than 150 days. In a more recent study (Cox, 1985, hereafter referred to as CX), the time-averaged results of a primitive equation, eddy resolving numerical simulation of the subtropical thermocline were presented. The time-dependent aspects of that solution will be considered here. The multilevel model of Bryan (1969), adapted to vectorizing computers by Cox (1984), is used. For a specific description of the model configuration and boundary conditions, refer to CX. The surface driving consists of an idealized wind-stress and Haney (1971) type differential heating, both constant in time. The variability which arises in the model solution is, therefore, not a result of variability in the boundary conditions.

Multiyear, basin scale undulations in the subtropics of the model solution will be presented in section 2, followed by an analysis of the undulations based upon planetary wave theory in section 3. Slowly propagating, zonal barotropic bands that arise in the solution will be presented and analyzed in section 4, and a general discussion of the results and their implications will follow in section 5.

2. Multiyear undulations in the subtropical gyre

The time-averaged results from the eddy resolving solution presented in CX were taken from years 18 to 24 of the experiment. The results presented in the present study are taken from the same 6-year interval, here identified as years 0 through 6. Shown in Fig. 1 is the instantaneous equivalent surface elevation (surface pressure converted to equivalent elevation) for all points south of the subtropical–subpolar gyre boundary, given at each half-year of the 6-year period. The contours represent geostrophic streamlines of flow at the ocean surface. The 6-year average of this quantity, shown as Fig. 3b of CX, presents a classical image of a Sverdrup gyre. The concentrated western boundary current and outflow is compensated by a broad southward drift in the interior and a westward return flow. The instantaneous maps, however, reveal that the southward transport in the model takes place in more concentrated flows that are highly variable in time. An example occurs at year 1.5, when two distinct southeastward flows are evident in the gyre interior. An inner one runs from roughly 20°E, 30°N to 35°E, 20°N, and an outer one from 40°E, 35°N to 50°E, 25°N thereafter becoming more disperse before joining the westward return flow. These two relatively narrow flows account for most of the required Sverdrup drift within the interior of the gyre. As time goes on, the two flows undergo a steady migration westward. At year 2.5 the inner flow has moved west of 20°E, and the outer one has begun a slow sweep southward and westward across the basin. By year 5.5 the latter has reached the position of the original inner flow, and a new outer flow has developed to the northeast.

The flow in the subsurface interior of the gyre is reflected by the "bowl" shape of the isopycnal surfaces there. The 6-year average depth of two such surfaces within the upper thermocline are shown in Fig. 2. The 25.5 sigma surface is the rough equivalent in the model to the 18-degree water of the North Atlantic subtropical gyre, with its primary ventilation in the western part of the gyre. Deeper isopycnals are ventilated further to the east along their outcrops, with the 26.0 surface being ventilated primarily to the east of 40°E. As in the case of sea surface height, the averaged shape of the bowl is relatively smoothly varying. However, patterns of the instantaneous depth, shown in Fig. 3 for the 25.5 surface, reveal steep and highly transient valleys and ridges. The bowl expands and contracts corresponding to the approximately 4-year undulation noted in the sea surface height field. At year 0.5, a zonally elongated valley has pushed from west to east along 25°N. As time goes on, the valley sweeps southward and collapses back to the west as a new cycle begins. At year 3.5, two sharp valleys have pushed eastward along the northwestern edge of the bowl. As the valleys move farther eastward and southward, a pattern similar to that at year 0.5 develops by year 4.5, with a subsequent migration to the west.

The cycle is evident at the 26.0 surface (Fig. 4) as well. At year 1.5, a valley extends to the east along 20°N, another valley is forming by ventilation along the outcrop to the north, and a ridge separates the two. By year 3.5, the southern valley has receded to the west, with only a remnant evident at 20°N, 20°E. The new valley sweeps southward until, at year 5.5, the pattern at year 1.5 is repeated. To obtain a clearer picture of the shape of the anomalies involved, the mean depth from Fig. 2 has been subtracted from the patterns of Fig. 4, and the result plotted in Fig. 5. The anomalies are basinwide and tend to be oriented along the outcrop at first formation. They undergo clockwise twisting as they sweep across the basin.

The vertical structure of the undulations is shown here in a series of sections along 24°N. The position of these sections within the gyre is shown by the dashed lines of Fig. 2. For reference, the field of density and potential vorticity averaged over six years are shown in Fig. 6. The averaged density pattern is dominated by the well-known east-to-west tilt of the thermocline, with mode waters lying above. Since relative vorticity is small compared to the Coriolis parameter f, and since f is constant in this section, the shape of the potential vorticity pattern is dictated by the local vertical gradient of density.

Instantaneous fields of density are shown in Fig. 7. The 26.0 surface, which was considered here, is indicated as the contour dividing the gray area from the white in the figure. At year 0.5, the eastern tip of the valley in the bowl of the 26.0 surface is seen at about 48°E where a frontlike structure exists through the vertical extent of the pycnocline. As time proceeds, the front moves westward until, at year 3.5, it is west of 10°E. A new front has developed to the east and the pattern of year 0.5 is repeated at year 4.5. The potential vorticity, shown in Fig. 8, tracks the development and movement of mode waters, indicated by white in the pattern. Shortly after ventilation occurs, depressing the entire thermocline along the outcrop, the mode, or low potential vorticity water formed there sweeps southward along isopycnals, arriving at the latitude of the section shown. At year 0.5, such a mode water has arrived in the eastern basin centered at about 42°E. It subsequently sweeps westward to join the permanent pool of low potential vorticity water that overlies the thermocline in the west. A new mass of mode water arrives in the east at around year 3.5 and the cycle repeats.

3. Modal analysis of the undulations

The east-to-west migration of the isopycnal surface depth anomalies in Fig. 5 strongly suggests the possibility that they are planetary Rossby waves. Their vertical coherence through the thermocline, shown in Fig. 7, further suggests that they are of low baroclinic mode number. The theoretical vertical profiles of the first

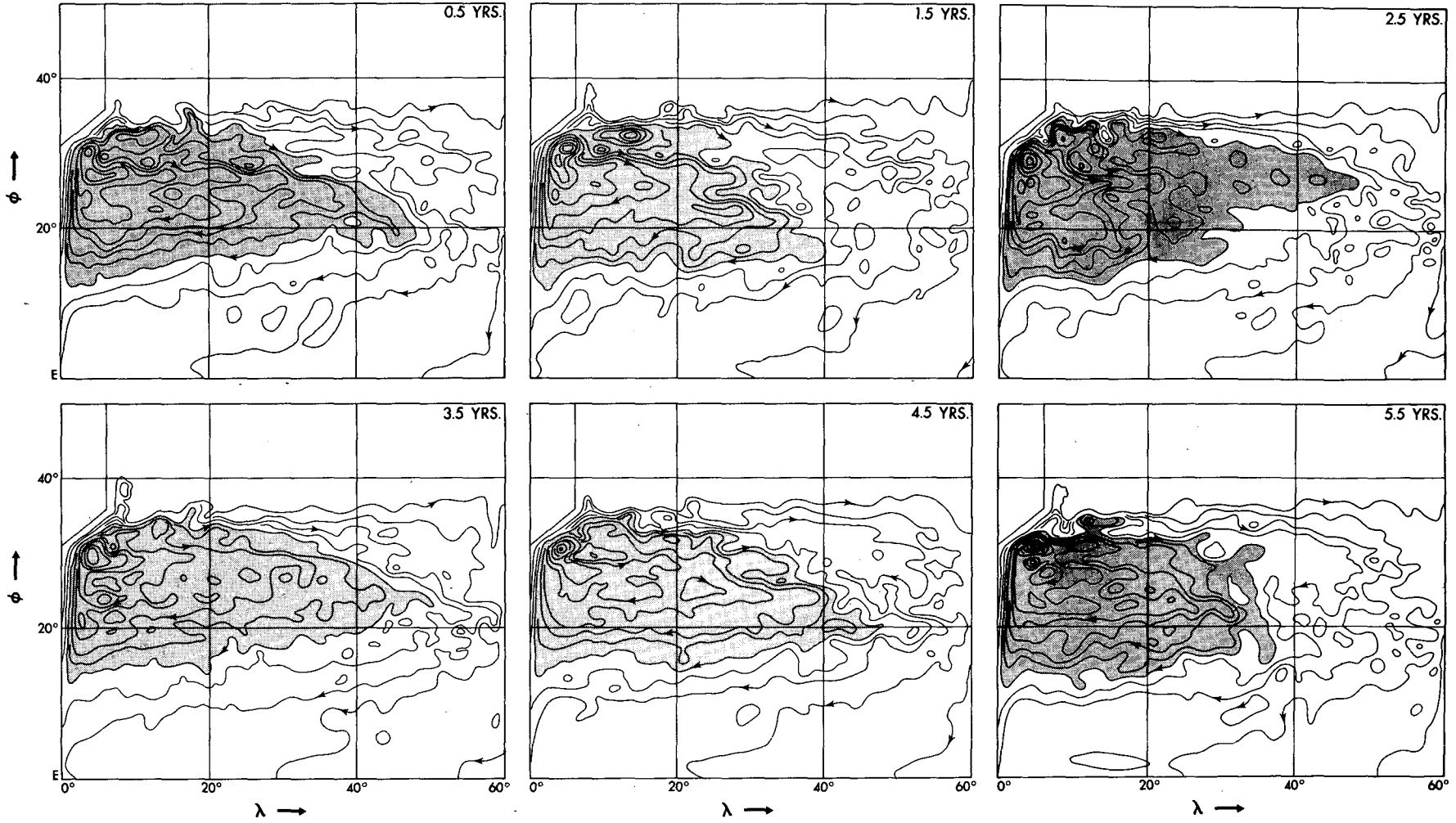

FIG. 1. Equivalent surface elevation at six points of time. Contour interval = 10 cm. The elevation is not drawn north of the subtropical-subpolar gyre boundary.

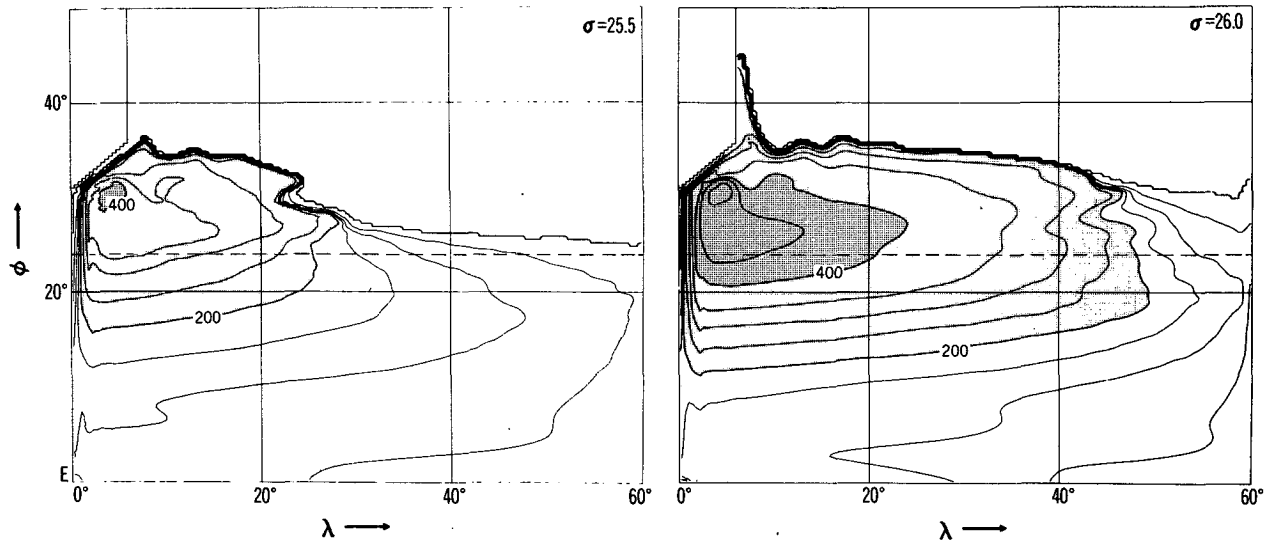

FIG. 2. The 6-year mean depth of two sigma surfaces in meters. The dashed line indicates 24°N for later reference.

and second modes have been plotted in Fig. 9 using the 6-year average vertical profile of density at three different longitudes along 24°N. The shapes change somewhat due to the east-to-west tilt of the thermocline. The first mode is of single sign vertically with a peak occurring at the approximate center of the thermocline. The second mode has one sign reversal, also near the center of the thermocline. To get a better idea of the vertical structure of the anomalies, the 6-year average density from Fig. 6 has been subtracted from the patterns of Fig. 7 and the results plotted in Fig. 10. Where the anomalies are strong, they are generally of single sign vertically, with a maximum which tracks downward to the west, in good agreement with the theoretically derived maximum of the first mode. There is also weak second and higher mode involvement, causing sign reversals, particularly where the signal is weak.

For internal Rossby waves whose zonal and meridional wavelengths are long compared to λ, the internal radius of deformation associated with the mode, the westward phase velocity of the wave is given by

$$C_{P_n} = -\beta\lambda_n^2 \qquad (1)$$

where β is the meridional gradient of the Coriolis force and n is the mode number. These quantities for the modes shown in Fig. 9 are given at the bottom of the figure. They range from approximately 4.6 cm s^{-1} in the east to 7.4 cm s^{-1} in the west for the first mode. These velocities are of the same general amplitude as the mean flow in the interior of the gyre according to Fig. 8 of CX. However, that figure also indicates that latitude 24°N is the approximate zero line in mean east–west velocity between eastward flow to the north and westward flow to the south. This can be verified to some degree from Fig. 1 of the present study as well. Advective alteration of the zonal propagation of the waves should, therefore, not be strong along this section.

The depth anomaly of the 26.0 surface along 24°N has been plotted against time in Fig. 11. Superimposed on this figure is a dashed line indicating, for each 20 degree band of longitude, the theoretical propagation velocity of the first baroclinic mode evaluated at the center of the band. The phase lines of the anomalies align reasonably well with the theoretically derived lines, lending additional evidence that the anomalies are primarily first baroclinic mode Rossby waves. The period of the undulations is seen from the figure to be 4 to 4.5 years.

It was noted earlier, in the discussion of Fig. 5, that the horizontal patterns of the anomalies show a tendency to rotate clockwise as they sweep westward. This may be explained by the advective effects of the mean gyral flow to the north and south of 24°N.

4. Zonal barotropic bands

There have been various reports from observational studies, of a tendency toward anisotropy in some transient flows, with decided zonal orientation. Richman et al. (1977), using moored current meter data taken during MODE I, find that their low frequency band (>100 day period) is dominated by zonal velocity fluctuations, primarily confined to the thermocline. Rossby et al. (1983), report various estimates of diffusivities derived from SOFAR floats in the western North Atlantic and find that zonal components generally exceed meridional components. Krauss and Böning (1987), using satellite-tracked buoys in the northern and eastern North Atlantic, also estimate larger zonal than meridional diffusivities. Yoshida (1970) reports evidence

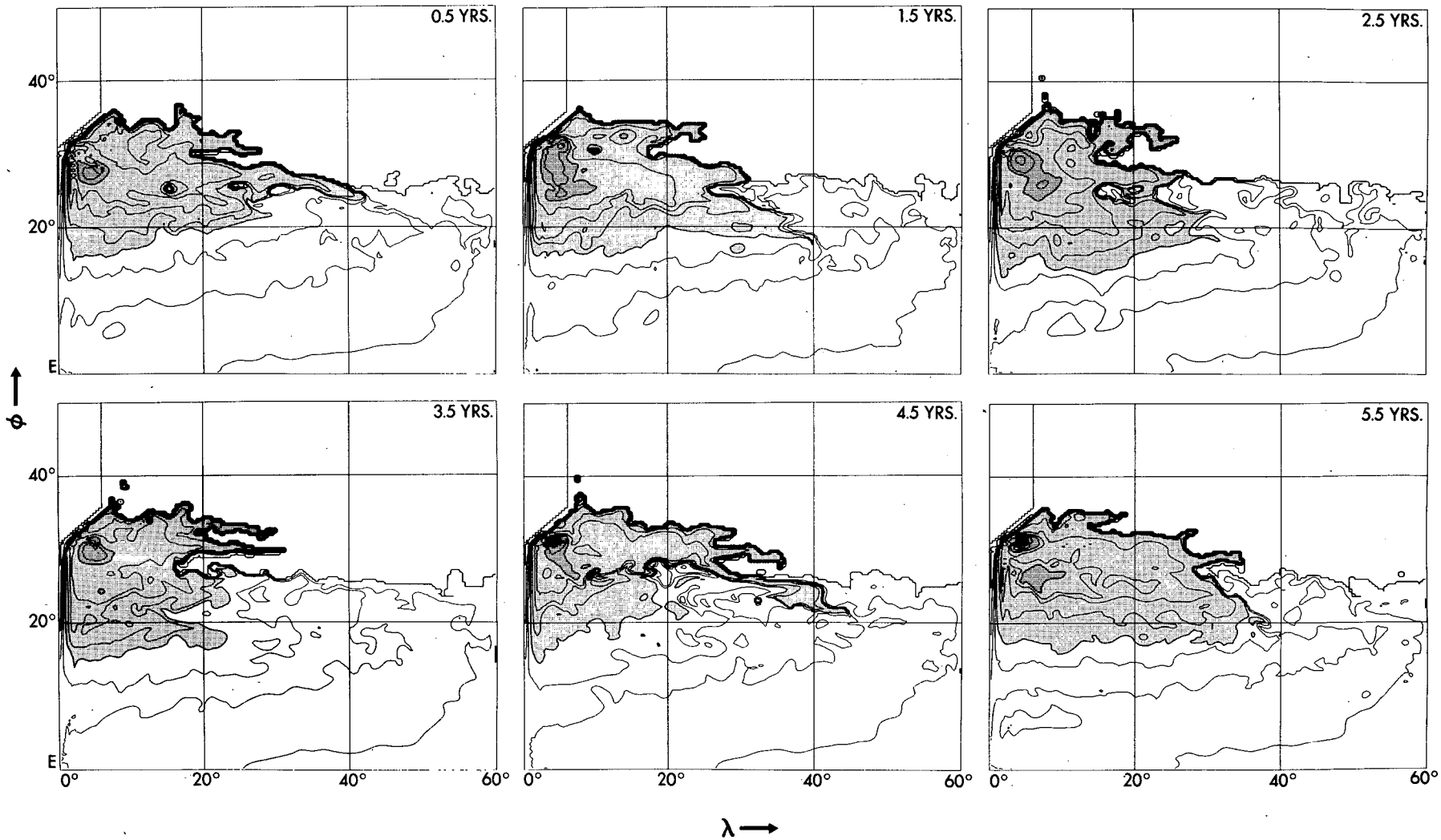

FIG. 3. Instantaneous depth of the 25.5 sigma surface at six points of time. The contour interval is 50 m with shading beginning at 200 m.

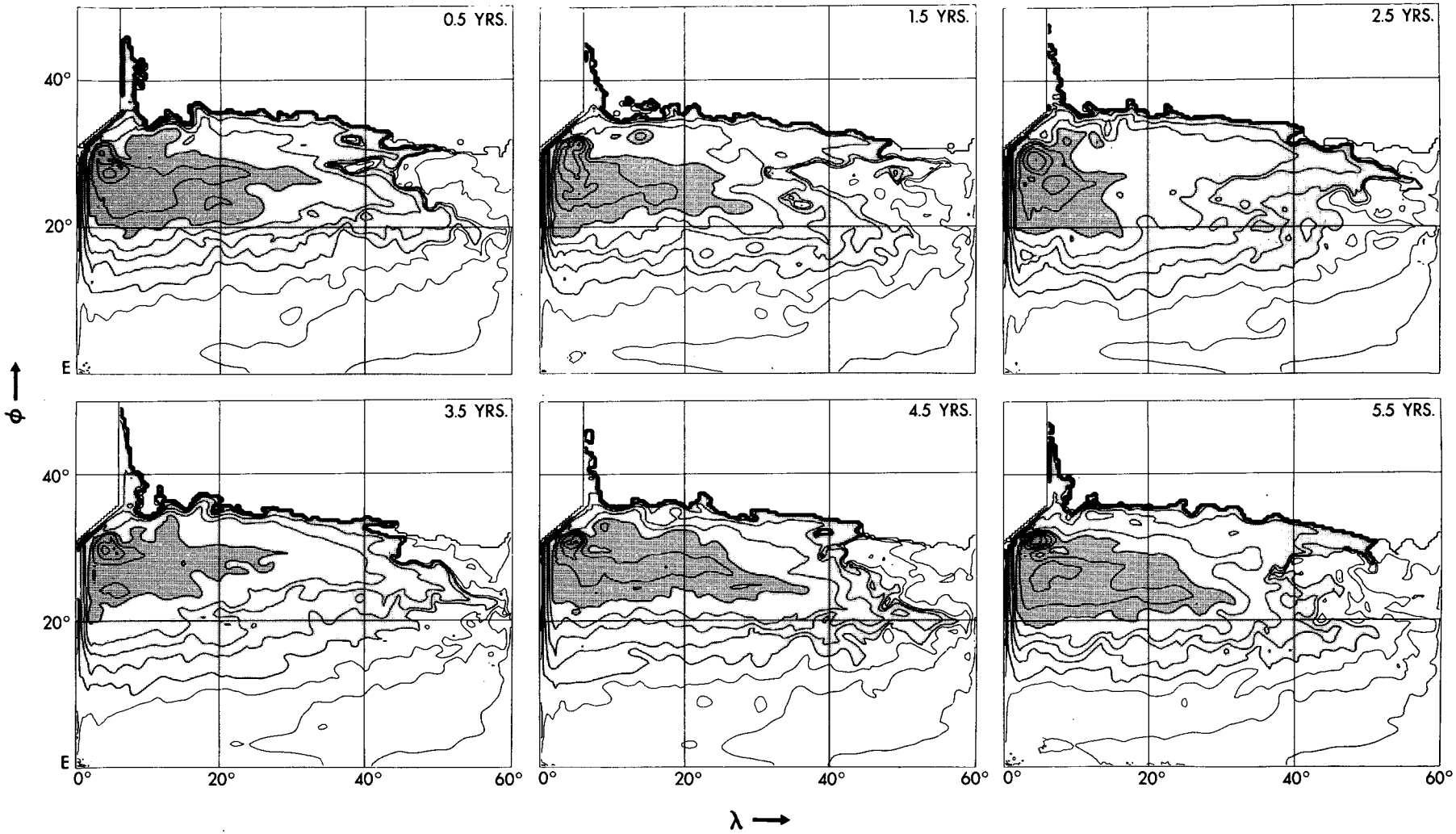

FIG. 4. As in Fig. 3 except for 26.0 sigma surface at six points of time. The contour interval is 50 m with shading beginning at 200 m.

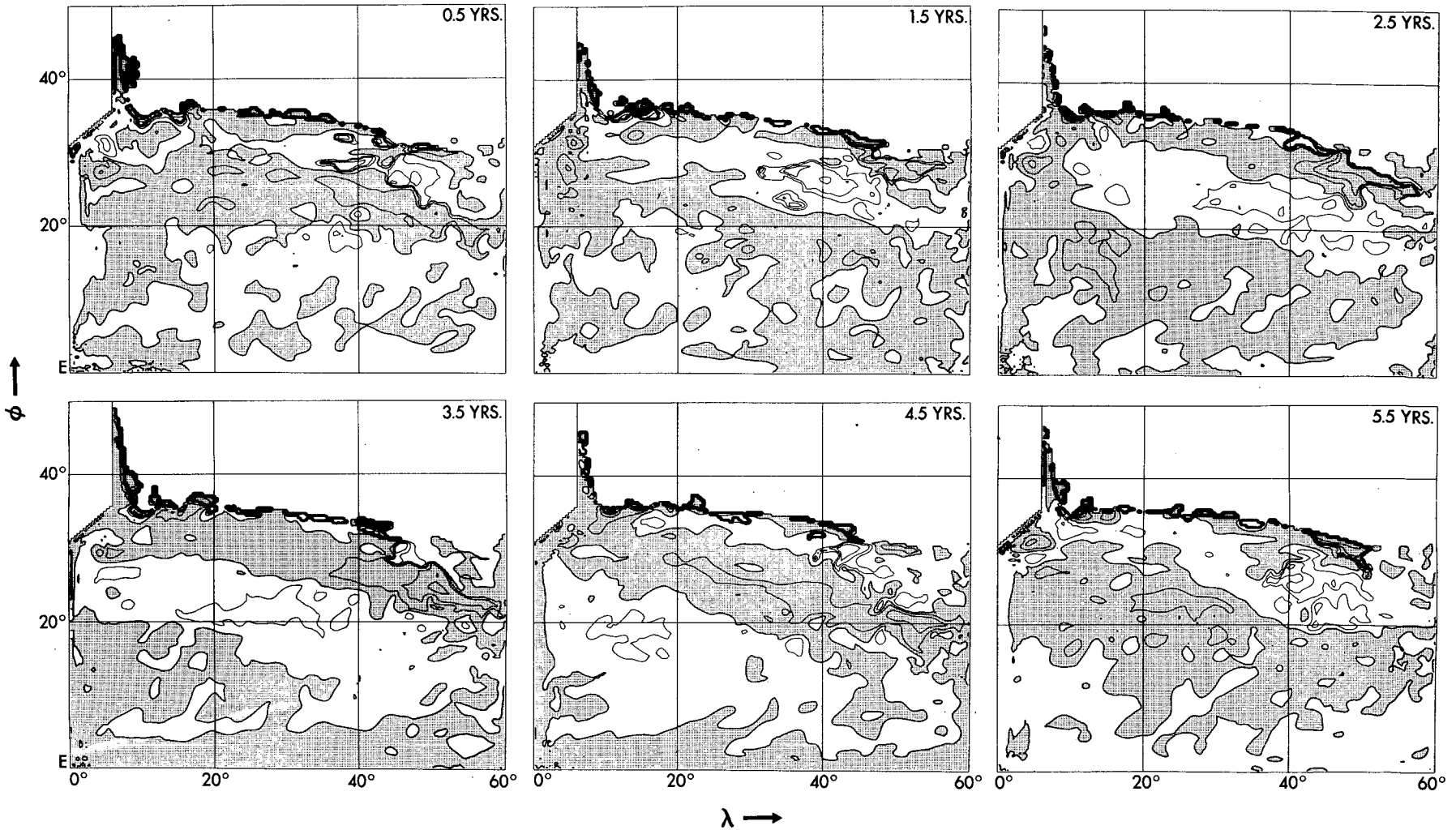

FIG. 5. Deviation of the depth of the 26.0 sigma surface from its 6-year mean at six points of time. The contour interval is 50 m with shading indicating shallower than the mean.

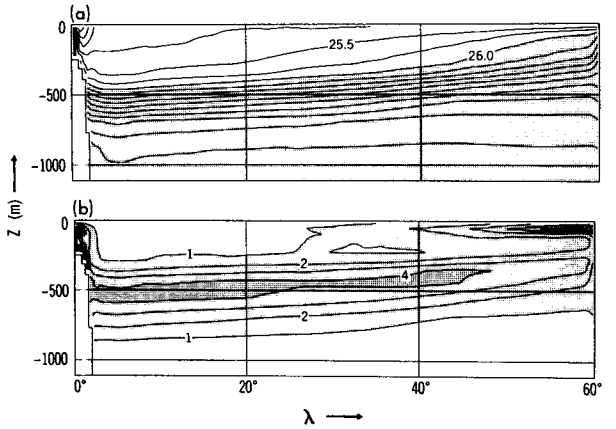

FIG. 6. The 6-year mean values of sigma (top) and potential vorticity (bottom) evaluated at 24°N. (See Fig. 2) Potential vorticity is in units of 10^{-12} cm^{-1} s^{-1}.

of long zonal bands in the u component of flow within the southwestern part of the North Pacific subtropical gyre. Hydrographic data taken within a few months across 28 degrees of longitude in this area are interpreted by the author as a series of meridionally alternating geostrophic jets, assuming a reference level at 2000 meters, with an apparent zonal scale larger than the region of measurement and a meridional scale of some 300 km.

Similar features are found in the present numerical solution. Estimates of eddy-induced diffusivity in the model indicate anisotropy, with zonal values exceeding meridional ones. Also, embedded in the mesoscale eddy field is a series of slowly propagating zonal jets similar to those reported in the North Pacific by Yoshida. These jets will be analyzed following a brief discussion of a possible theoretical basis for the observed anisotropy.

Rhines (1977) summarizes a theory of geostrophic turbulence, originating with the early work of Batchelor (1953) and proceeding through the work of Rhines (1975) and others, in which eddy energy entering the barotropic mode of a flat-bottomed ocean will tend to cascade to large zonal scales, producing a series of east–west jets. The meridional scale is found to be given by $k = (\beta/2U)^{1/2}$ where β is the meridional gradient of the Coriolis force and U is rms particle speed. Furthermore, energy originating in baroclinic modes is found to cascade first to the deformation radius, after which it has a tendency to proceed to the barotropic mode. A scenario is established, therefore, in which eddy energy arising from mechanisms such as shear instability or baroclinic instability can find its way eventually into elongated zonal barotropic bands of flow. The point is made that any of several circumstances, including inhomogeniety of the eddy energy and the presence of bottom topography, can prevent the process from going to completion.

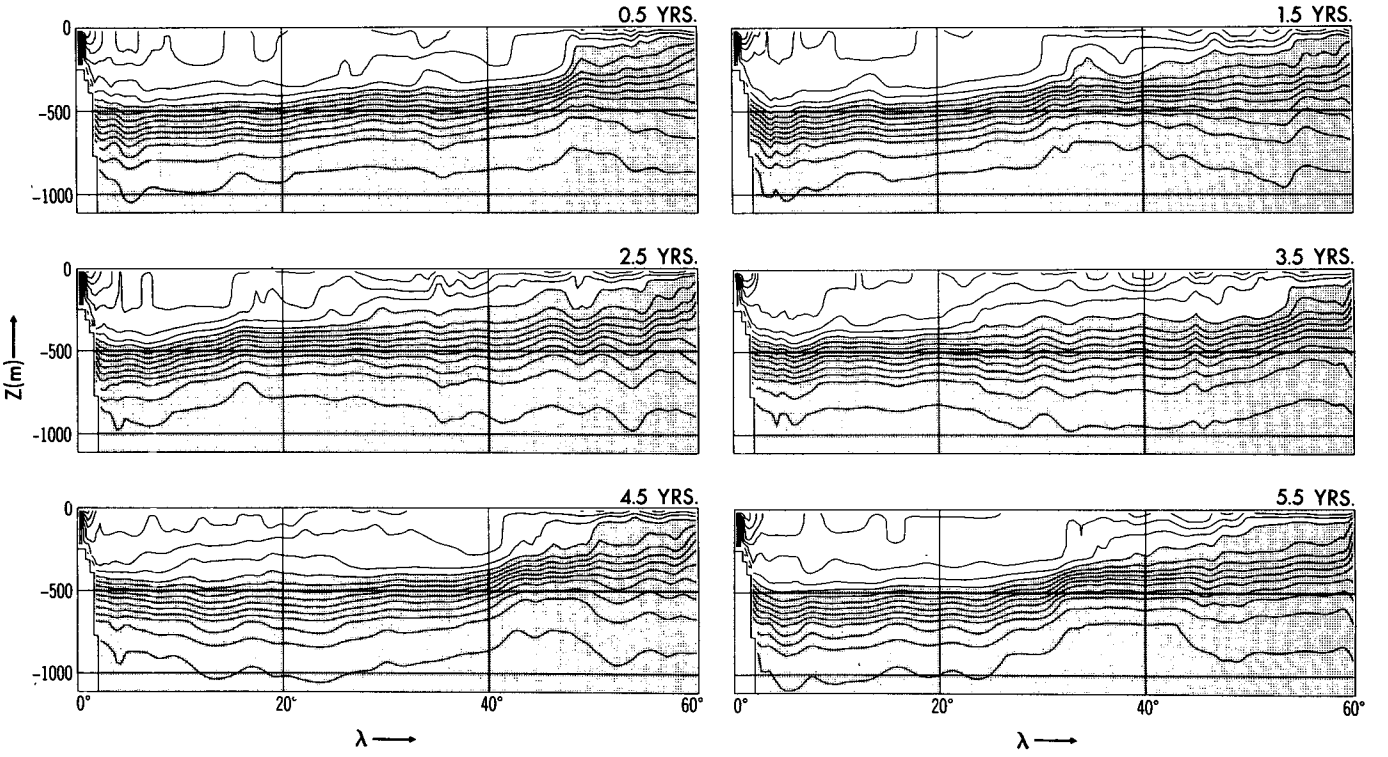

FIG. 7. Instantaneous values of sigma at 24°N for six points of time. The contour interval is 0.25 with shading beginning at sigma = 26.0.

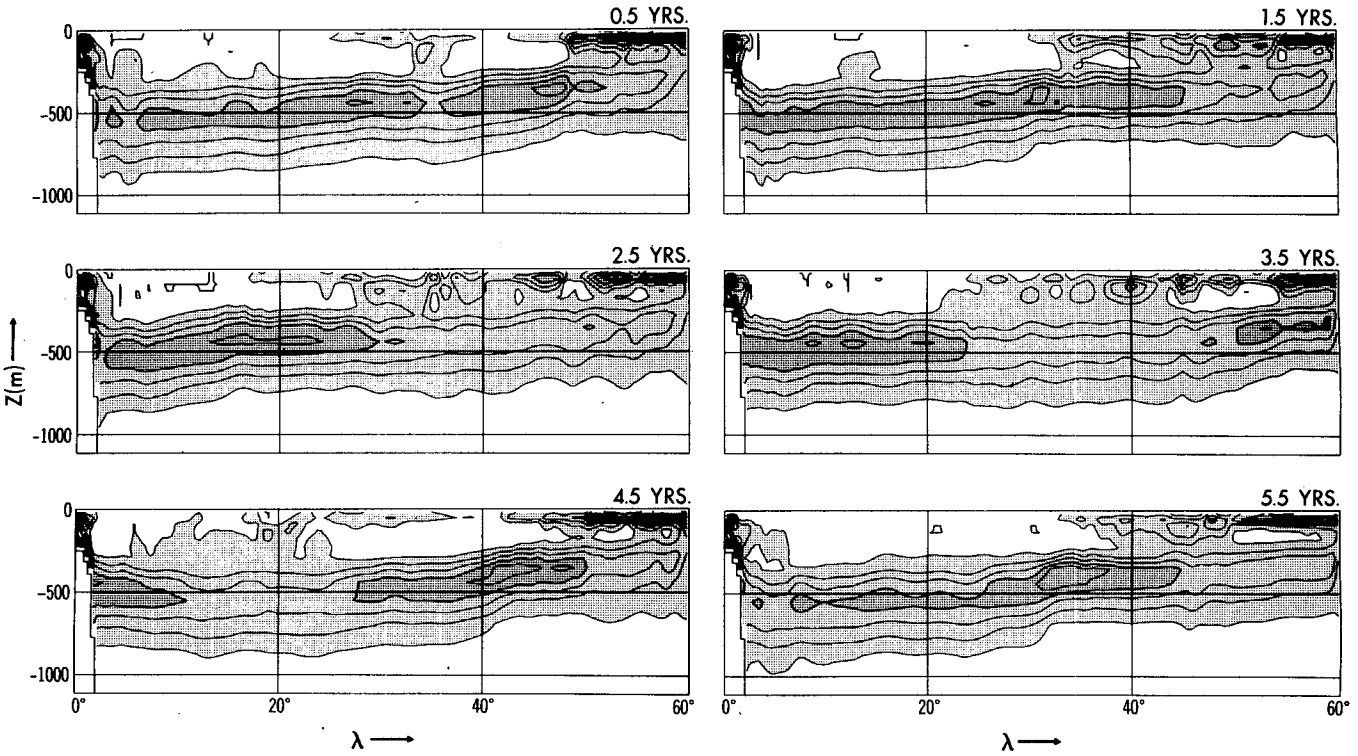

FIG. 8. Instantaneous values of potential vorticity at 24°N for six points of time. The contour interval is 1×10^{-12} with stippling beginning at 1×10^{-12} in units of $cm^{-1}\ s^{-1}$.

Since the passage of energy through the barotropic mode is central to the theory presented by Rhines, this mode has been analyzed in the model. Isolines of the horizontal mass transport stream function, a prognostic variable of the model, represent streamlines of barotropic flow. They are plotted in Fig. 12a at year 5.5 in the solution, with the 6-year average subtracted out to leave only the time-variant component. A cursory look at this pattern shows a series of essentially isotropic mesoscale eddies. These eddies are similar in horizontal scale to the eddy structure found above the thermocline that is discussed in CX. In that study, the eddies were

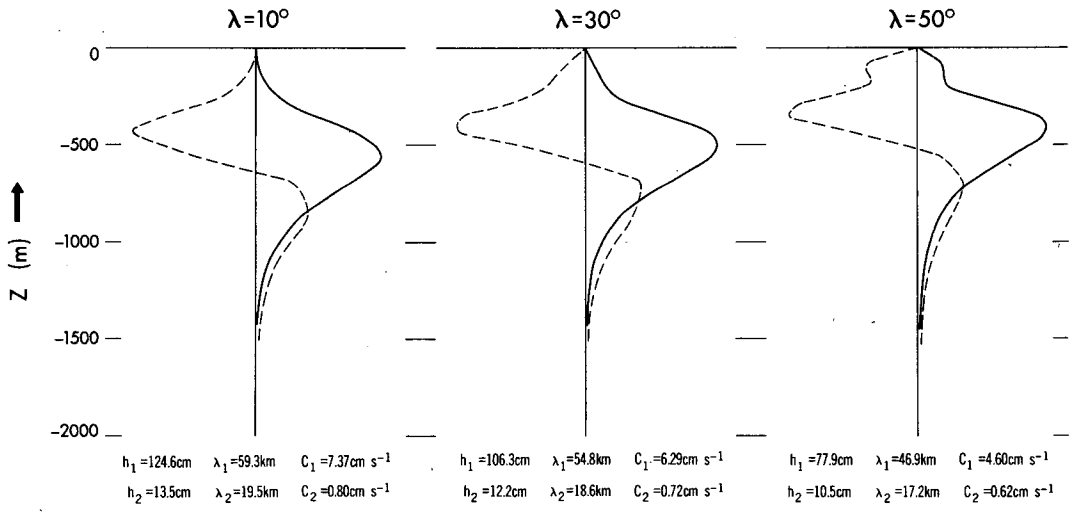

FIG. 9. Vertical profile of the first (solid) and second (dashed) baroclinic modes evaluated from the density data of Fig. 6 averaged over three 20 degree bands of longitude centered at 10°E, 30°E and 50°E. The equivalent depths, radii of deformation and westward phase velocities are given below.

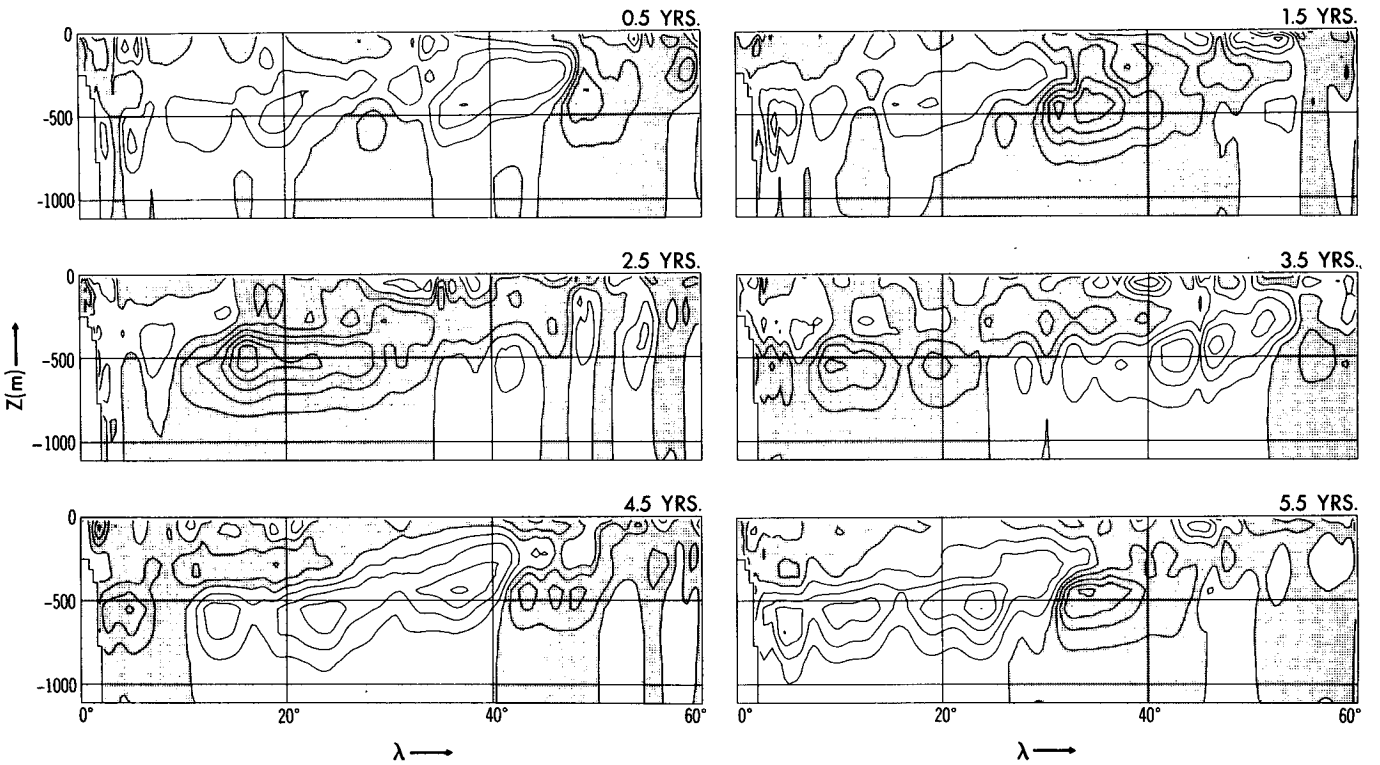

FIG. 10. Instantaneous values of the deviation of sigma from its 6-year mean at 24°N for six points of time. The contour interval is 0.125 with shading indicating more dense than the mean.

identified as being primarily first baroclinic modal, and generated by baroclinic instability within the westward return flow of the subtropical gyre. Their presence in the barotropic mode is evidence that the first phase of the scenario suggested here is occurring. Energy is, in fact, being transferred from the first baroclinic mode into the barotropic mode at the horizontal scale of the deformation radius of the first baroclinic mode.

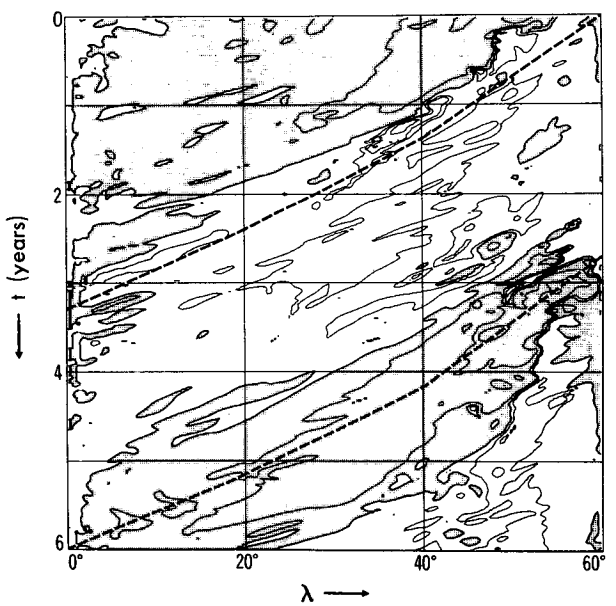

FIG. 11. Deviation of the depth of the 26.0 sigma surface from its 6-year mean along 24°N. The contour interval is 50 m with shading indicating shallower than the mean. The dashed lines represent the theoretical first baroclinic mode phase velocities from Fig. 9.

The time series of the time variant component of the stream function has been low-pass filtered using a Hamming digital filter with a Lanczos window (Hamming, 1977), and the results plotted for year 5.5 in Fig. 12b. The transfer function of the filter is shown in Fig. 13. Variation of period shorter than about four months is blocked by the filter. This eliminates the mesoscale eddies, which are of roughly 50-day period. Remaining are a series of zonally elongated gyres throughout the basin, but with greatest amplitude in the area where the strongest mesoscale eddies exist in Fig. 12a. Note that these zonal jets in the barotropic mode end abruptly at the base of the idealized continental rise, which begins some 4 degrees of longitude out from the western boundary. Their presence is evidence that the second phase of the scenario, the passage of barotropic energy into low zonal wave numbers, is also occurring.

To obtain an idea of the nature of the bands, the filtered data has been plotted against time along longitude 20°E in Fig. 14. Where the bands are strongest, in the subtropical gyre, the phase propagation is southward with a period of approximately 1.1 year and a meridional wavelength of 470 km. A typical rms particle speed taken from Fig. 12a is 5 cm s^{-1} [approxi-

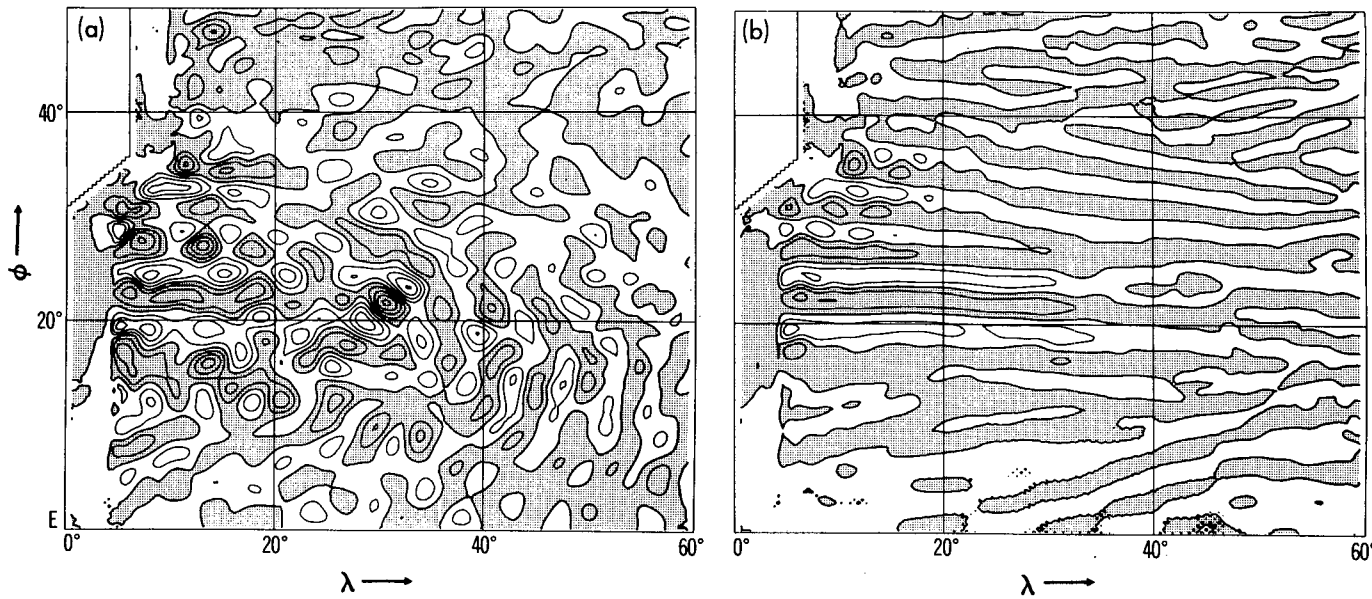

FIG. 12. Deviation of the horizontal mass transport stream function from its 6-year mean at year 5.5. (a) Unfiltered, (b) filtered with transfer function of Fig. 13. Contour interval is 20 Sv.

mately 20 Sv (Sv ≡ 10^6 m^3 s^{-1}) per degree latitude in the figure.] If this value is used in the formula presented in the theory above, one obtains a wavelength of approximately 440 km, in good agreement with that observed in the model. Further, if the period of 1.1 year and wavelength of 470 km are inserted into the dispersion relation for barotropic Rossby waves, one obtains a zonal wavelength of approximately 4000 km, and a group velocity of about 11 cm s^{-1} westward and 3 cm s^{-1} northward. Such an orientation of the energy vector will cause the eddy energy, originally generated by baroclinic instability in the westward return flow, to make its way eventually into the interior of the western region of the subtropical gyre in the form of zonal barotropic bands. The placement of the most intense jets in Fig. 12b seems to substantiate this interpretation.

5. Summary and conclusions

The numerical solution of the primitive equations for a box ocean with relatively low mixing coefficients

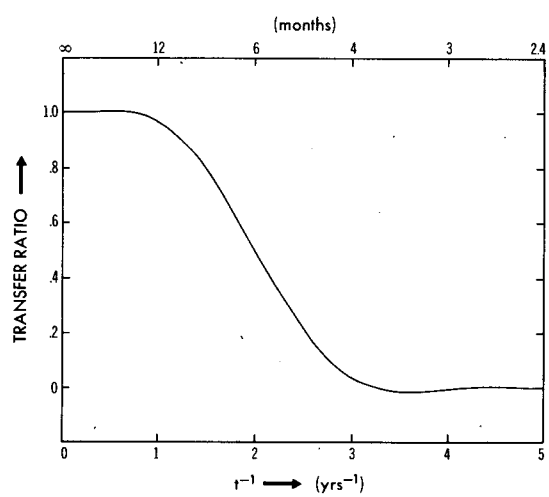

FIG. 13. Transfer function of filter used in Fig. 12. Filter used is a digital Hamming type with Lanczos window.

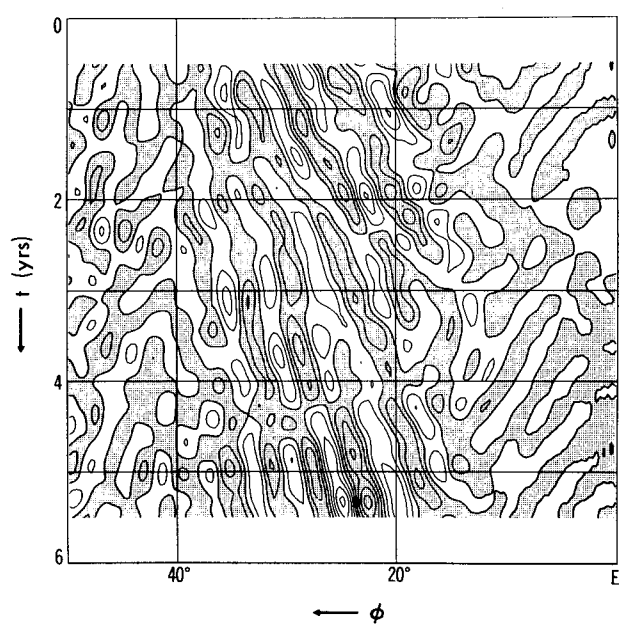

FIG. 14. Filtered deviation of the horizontal mass transport stream function from its 6-year mean evaluated at 20° longitude. Contour interval is 10 Sv.

exhibits time dependence of three primary scales. These scales do not arise from the imposed boundary conditions which are temporally constant. Besides the well-known mesoscale variability of approximately 50-day period, zonal barotropic bands of 1.1 year period and gyre scale undulations of 4 to 4.5 year period have significant signatures in the solution. The latter are shown to be baroclinic and of the first mode primarily. Their manifestation in the circulation pattern of the subtropical gyre is such that the equatorward transport, which is required throughout the interior of the gyre by Sverdrup theory, is realized not in the classical sense of a broad, sluggish drift, but as a series of concentrated equatorward flows which proceed from east to west across the gyre at the speed of the first baroclinic mode. In alternate terms, the undulations may be described as occurrences of ventilation along isopycnal outcrops on the poleward side of the gyre producing depressions in the main thermocline, and subsequent propagation (distorted by gyral advection) of the disturbances southward and westward through the gyre.

In CX it was shown that baroclinic instability within the westward return flow of the subtropical gyre is set off by the intrusion of low potential vorticity waters into the interior of the gyre from outcropping regions. The north–south minimum in potential vorticity that is produced in this process satisfies well-known conditions for the onset of baroclinic instability. It follows that if the ventilation undulates in time, the observed baroclinic instability in the westward return flow may be expected to do so as well. Amplitudes of eddy energy in this region verify that such a relationship is occurring in the model. Perhaps the much predicted baroclinic instability in this region of the North Atlantic has been observed only sporadically owing to interannual temporal variations.

What sets the period of the undulations remains an open question, although one scenario is strongly suggested by the solution. The onset of a new ventilation event along the outcrops appears to follow promptly the arrival at the western boundary of the Rossby wave initiated by the previous ventilation event. Thus, a circular process is suggested in which the energy within the undulation is, upon its arrival at the western boundary, transferred relatively quickly back to the outcrop region where a new Rossby wave is formed. There are two possible mechanisms to accomplish this. The transfer may be advective in nature, with the western boundary current and its eastward extension carrying the signal in clockwise fashion back to the outcrop. Or a linear process may be involved, in which coastal and equatorial internal Kelvin waves return the energy to the east in a counterclockwise fashion. The velocity of energy transfer in either of these scenarios is sufficient to produce the relatively quick reappearance of the energy at the outcrop after the Rossby wave has arrived at the western boundary. The advective path would have a velocity of that of the western boundary current, 1–2 m s^{-1}, whereas the linear path would be even faster, 3 m s^{-1}, for the first baroclinic mode equatorial Kelvin wave, although the latter has somewhat longer path length. These compare to the 5–10 cm s^{-1} group velocity of the Rossby wave segment of the path.

There is evidence in Fig. 5 that some multiyear energy is passing along the equator. The 26.0 sigma surface there rises and falls slightly with the arrival of the Rossby wave at the western boundary to the north. The amplitude of the signal at the equator is smaller than that of the Rossby wave, as is expected due to the high group velocity of the equatorial Kelvin wave. Unfortunately, it has proven difficult to examine the solution for either of these two scenarios, primarily because of the very high energy flux velocities involved. The wave signal, easily identified in the east-to-west phase (e.g., Fig. 10), becomes highly stretched by the acceleration it undergoes in the west-to-east phase of its path. This, together with the presence of relatively energetic signals at higher frequencies which have a camouflaging effect, has made the passage of energy in the multiyear signal difficult to detect in the west-to-east phase. To investigate this mechanism more fully, either a more sophisticated energy flux analysis than that used here, or a separate study using a more appropriate model, will have to be carried out.

Assuming the time taken for the return phase of the undulation signal is small compared to the Rossby wave phase, the period can be estimated by

$$T = L/\beta\lambda_1^2 \tag{2}$$

where L is the basin width and the denominator is the average speed of the first baroclinic Rossby wave.

It was noted earlier that there are few sets of observed data that extend sufficiently long in time to enable one to detect multiyear signals of the type described from the model. One set which is available, however, is the Panulirus data taken near Bermuda. A spectral analysis of the fluctuations in temperature taken from this dataset has been carried out by Frankignoul (1981). The spectra at different levels are generally red between 2 and 12 year periods, the latter being the low frequency cutoff of the study, and show no peaks in that interval. However, a plot of the annual mean depth of the 4 degree isotherm at Panulirus by Roemmich and Wunsch (1984), reproduced here in Fig. 15, reveals distinct episodes of vertical movement at varying multiyear intervals. Whether some of these may be gyre-scale undulations of the type described from the model cannot be determined without similar data from other parts of the gyre.

The episodic, rather than periodic, nature of the observed signal may not in itself eliminate the possibility that it is a similar phenomenon to that in the model. Long-term variations in surface wind or buoyancy driving may alter the signal sufficiently in the ocean, particularly via convection along the ventilation region

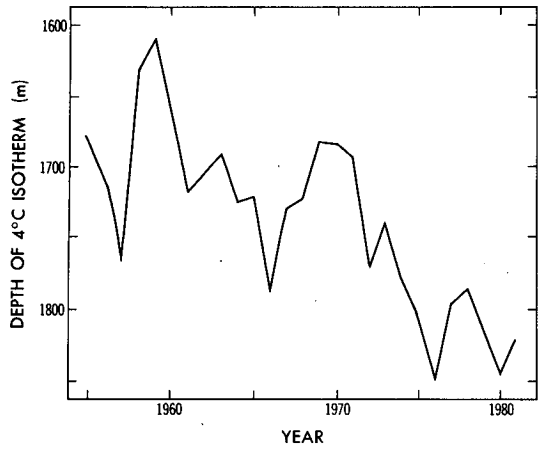

FIG. 15. Depth of the 4 degree isotherm from the Panulirus data set taken near Bermuda, reproduced from Roemmich and Wunsch (1984).

in the northeastern segment of the gyre, to yield an episodic type of behavior. Perhaps the most important point to be made from the model solution is that gyre-scale undulations of the multiyear period are possible in the most simply driven form of the primitive equations, and should be considered a potential source of variability in any midlatitude analysis.

The zonal barotropic bands generated in the model solution play a significant role in the mixing of potential vorticity and tracer reported in CX for the present model. It was noted earlier that dispersion calculations done on the present solution indicate greater zonal than meridional effective diffusivities due to time-variant flow. Much of the enhanced mixing reported in CX derives, apparently, from zonal velocity fluctuations. The importance of the zonal bands to the dynamics of the real ocean must, however, remain in some doubt. This is due primarily to the use of a flat bottom in the model, a simplification which may have significant influence on the barotropic mode. It was pointed out earlier that the bands in Fig. 12b end abruptly at the base of the idealized continental rise, the only topographic feature present in the model basin. The question arises as to whether the bands would be generated at all if more realistic topography were used.

The zonally oriented velocity fluctuations found by Richman et al. (1977) are primarily confined to the thermocline region, indicating a more baroclinic than barotropic nature. The zonal jets of Yoshida (1970) also possess a significant baroclinic component. If the process of zonal elongation must occur in the barotropic mode, how can energy return to the baroclinic mode? One possible scenario is that barotropic bands may be generated in flat-bottomed regions of the ocean, after which their energy is converted into baroclinic modes by topographic influences as their group propagates westward. Another possibility is nonlinear intermodal energy exchanges. Work is currently under way by C. Böning, in which topography is introduced into the interior of the model basin to evaluate its effect on the bands and the nature of the eddy-induced mixing in general.

Acknowledgments. The author wishes to thank Kirk Bryan, Claus Böning, and Peter Rhines for valuable discussions on the analysis of the results. Thanks also to Kim Reed, Phil Tunison and Cathy Raphael for help in preparing the figures.

REFERENCES

Batchelor, G. K., 1953: *Homogeneous Turbulence,* Cambridge University Press, 197 pp.

Bryan, K., 1969: A numerical method for the study of the circulation of the World Ocean. *J. Comput. Phys.*, **4,** 347–376.

Cox, M. D., 1984: A primitive equation, 3-dimensional model of the ocean. GFDL Ocean Group Tech. Rep. No. 1, 143 pp.

——, 1985: An eddy resolving numerical model of the ventilated thermocline. *J. Phys. Oceanogr.*, **15,** 1312–1324.

Frankignoul, C., 1981: Low-frequency temperature fluctuations off Bermuda. *J. Geophys. Res.*, **86,** 6522–6528.

Hamming, R. W., 1977: *Digital Filters,* Prentice Hall, 226 pp.

Haney, R. L., 1971: Surface thermal boundary condition for ocean circulation models. *J. Phys. Oceanogr.*, **1,** 241–248.

Holland, W. R., 1978: The role of mesoscale eddies in the general circulation of the ocean—numerical experiments using a wind driven quasi-geostrophic model. *J. Phys. Oceanogr.*, **8,** 363–392.

Krauss, W., and C. Böning, 1987: Lagrangian properties of eddy fields in the northern North Atlantic as deduced from satellite-tracked buoys. Submitted for publication.

Price, J. M., and L. Magaard, 1980: Rossby wave analysis of the baroclinic potential energy in the upper 500 M of the North Pacific. *J. Mar. Res.*, **38,** 249–264.

Rhines, P. B., 1975: Waves and turbulence on a beta-plane. *J. Fluid Mech.*, **69,** 417–443.

——, 1977: The dynamics of unsteady currents. *The Sea,* Vol. 6, Wiley Interscience, 189–318.

Richman, J. G., C. Wunsch and N. G. Hogg, 1977: Space and time scales of mesoscale motion in the western North Atlantic. *Rev. Geophys. Space Phys.*, **15,** 385–420.

Robinson, A. R. (ed.), 1983: *Eddies In Marine Science.* Springer-Verlag, 609 pp.

Roemmich, D., and C. Wunsch, 1984: Apparent changes in the climatic state of the deep North Atlantic Ocean. *Nature,* **307,** 447–450.

Rossby, H. T., S. C. Riser and A. J. Mariano, 1983: The western North Atlantic—a Lagrangian viewpoint. *Eddies In Marine Science,* A. R. Robinson, Ed., Springer-Verlag, 66–91.

White, W. B., and J. F. T. Saur, 1983: Sources of interannual baroclinic waves in the eastern subtropical North Pacific. *J. Phys. Oceanogr.*, **13,** 531–544.

Yoshida, K., 1970: Subtropical countercurrents: band structures revealed from CSK data. *The Kuroshio,* J. C. Marr, Ed., East-West Center Press, 197–204.